IMMUNOLOGY

Rapid, site-specific labeling of "off-the-shelf" and native serum autoantibodies with T cell–redirecting domains

Fabiana Zappala[1], Elizabeth Higbee-Dempsey[1], Bian Jang[1], Joann Miller[2], Lesan Yan[1], Nicholas G. Minutolo[3], Gabriela T. Rosado González[4], Andrew Tsourkas[1]*, Burcin Altun Ozdemir[1]*

Extensive antibody engineering and cloning is typically required to generate new bispecific antibodies. Made-to-order genes, advanced expression systems, and high-efficiency cloning can simplify and accelerate this process, but it still can take months before a functional product is realized. We developed a simple method to site-specifically and covalently attach a T cell–redirecting domain to any off-the-shelf, human immunoglobulin G (IgG) or native IgG isolated from serum. No antibody engineering, cloning, or knowledge of the antibody sequence is required. Bispecific antibodies are generated in just hours. By labeling antibodies isolated from tumor-bearing mice, including two syngeneic models, we generated T cell–redirecting autoantibodies (TRAAbs) that act as an effective therapeutic. TRAAbs preferentially bind tumor tissue over healthy tissue, indicating a previously unexplored therapeutic window. The use of autoantibodies to direct the tumor targeting of bispecific antibodies represents a new paradigm in personalized medicine that eliminates the need to identify tumor biomarkers.

INTRODUCTION

Bispecific antibodies (BiAbs) have emerged as a promising cancer treatment, with a growing list of encouraging clinical results (*1*, *2*). BiAbs enable the binding of two separate targets or the binding of two distinct sites on the same target, simultaneously. This can have important implications when applied as a therapeutic, such as improved specificity and/or unique biological effects (*3–6*). In one common application, BiAbs are designed to physically bring T cells and cancer cells closer together to enhance the immune clearing of cancer cells. Demonstrating the promise of T cell–redirecting BiAbs, blinatumomab, an anti-CD3 × anti-CD19 pair, has produced clinical remission in precursor B cell acute lymphoblastic leukemia at thousand-fold lower dosages than rituximab (anti-CD20 monoclonal antibody), without needing a secondary T cell costimulatory signal (*7–9*). Similarly, catumaxomab [anti-CD3 × anti-EpCAM (Epithelial Cell Adhesion Molecule)] has led to clinical benefit in patients with malignant ascites at a dose totaling 230 µg over 11 days (*3*, *10–12*). In contrast, conventional antibody therapies require cumulative antibody doses ranging from 5 to 20 g per patient over the course of months to years (*13*).

Many BiAb formats have been developed, but the generation of highly uniform BiAbs generally requires extensive antibody engineering or cloning up front, due to the low yields and purity of forming BiAbs by chemical cross-linking techniques (*14*) and the limited versatility and applicability of species-restricted pairing (e.g., Triomab) (*13*, *15–17*). Although made-to-order genes, advanced expression systems, and high-efficiency cloning techniques speed up and simplify the creation of BiAbs, it can still take months to make each new BiAb construct. Issues like loss of specificity, aggregation,

light-chain swapping, and heterogeneity can further slowdown this process, and additional time and expertise are required when exact antibody sequences are unknown and must still be determined. This creates a barrier for entry into this field for many laboratories and slows down the productivity of others. A methodology that produces functional BiAbs from off-the-shelf immunoglobulin G (IgG) or native antibodies from serum or culture, without the need for antibody engineering and cloning, could offer unique opportunities to accelerate BiAb research and enable previously unexplored therapeutic paradigms.

Here, we describe a simple method to attach an anti-CD3–targeting domain site-specifically and covalently to the heavy chains of any off-the-shelf, full-length IgG. This approach to making BiAbs does not require antibody engineering, cloning, or modifications, thus reducing the BiAb production time from months to hours. Our technique uses a photoreactive antibody–binding domain (pAbBD) that is derived from the small (~6.5-kDa), thermally stable HTB1 domain of a version of protein G that only binds to the Fc region of antibodies (*18*). Our laboratory has engineered this pAbBD to contain a photoreactive unnatural amino acid in the Fc-binding site (*19*). The photoreactive amino acid within the pAbBD domain creates a covalent link between a pAbBD–anti-CD3 fusion protein and an IgG of interest to prevent dissociation (Fig. 1A). This technique allows control over the number of modifications per IgG molecule and results in uniform antibody conjugates in high yields.

BiAbs were produced from a range of clinically approved IgGs, and their functionalities were examined to demonstrate the method's ease and utility. Furthermore, we tested whether a living subject's endogenous antibodies can be transformed into bispecific T cell–redirecting autoantibodies (TRAAbs) and used to enhance the immune system's ability to specifically suppress and/or eradicate malignant cells.

RESULTS

Rapid production of BiAbs

To enable the rapid functionalization of antibodies, namely, IgG, with T cell–redirecting domains, we created fusion proteins composed of pAbBDs and anti-CD3–targeting domains (Fig. 1A). The

[1]Department of Bioengineering, University of Pennsylvania, 210 S. 33rd Street, 240 Skirkanich Hall, Philadelphia, PA 19104, USA. [2]Department of Radiation Oncology, Perelman School of Medicine, University of Pennsylvania, 3400 Civic Center Blvd, Philadelphia, PA 19104, USA. [3]Department of Pathology and Laboratory Medicine, Perelman School of Medicine, University of Pennsylvania, 3400 Civic Center Blvd, Philadelphia, PA 19104, USA. [4]Gabriela T. Rosado González, Department of Chemistry, University of Puerto Rico, 14, 2534 Av. Universidad Ste. 1401, San Juan, 00925 Puerto Rico.
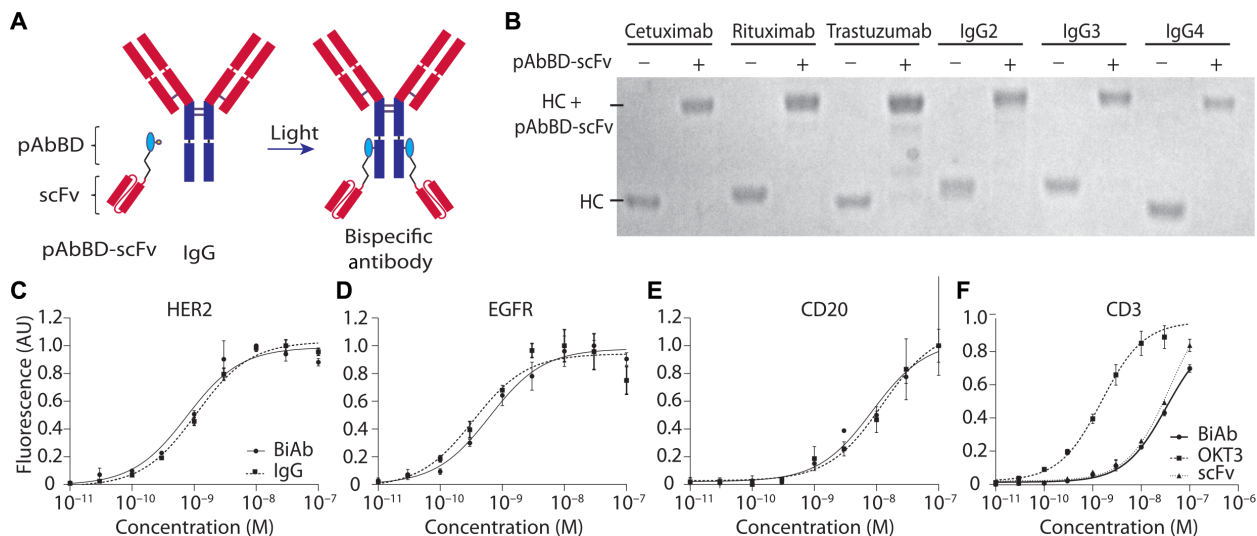*Corresponding author. Email: atsourk@seas.upenn.edu (A.T.); burcin.altun.upenn.edu (B.A.O.)

Fig. 1. BiAb production mediated by a pAbBD results in six different, pure constructs that bind their respective tumor targets as expected. (**A**) An anti-CD3 scFv was fused with a pAbBD. Two hours of irradiation with nondamaging long-wavelength ultraviolet (UV) light induces covalent attachment of the fusion protein to the IgG Fc region. (**B**) Six human antibodies—rituximab, cetuximab, trastuzumab, IgG2, IgG3, and IgG4—and the resulting BiAbs produced by photocrosslinking with pAbBD–anti-CD3 fusion protein were analyzed on a reducing SDS–polyacrylamide gel electrophoresis (SDS-PAGE). Unbound, excess pAbBD-scFv was removed via filtration. The bands represent IgG heavy chains (HC) before and after photocrosslinking. (**C** to **E**) HER2$^+$ T617, epidermal growth factor receptor–positive (EGFR$^+$) MDA-MB-468, and CD20$^+$ HT1080 cell lines were seeded, fixed, and blocked with normal goat serum. Binding curves of photocrosslinked (C) anti-HER2 (trastuzumab) × anti-CD3, (D) anti-EGFR (cetuximab) × anti-CD3, and (E) anti-CD20 (rituximab) × anti-CD3 BiAbs and the respective monospecific antibodies from which they were derived were obtained after incubation with a fluorescent secondary antibody. Fluorescence intensity was measured using a plate reader. The dissociation constant (K_d) values were (A) 0.9 nM for the BiAb and 1.16 nM for monoclonal antibody, (B) 0.60 nM for the BiAb and 0.49 nM for the monoclonal antibody, and (C) 8.2 nM for the BiAb and 12 nM for the monoclonal antibody. All coefficient of determination (R^2) values are greater than 0.9. (**F**) Human T cells were incubated with serial dilutions of anti-EGFR × anti-CD3 scFv BiAb, free anti-CD3 scFv, and positive control OKT3, and binding was measured via flow cytometry. The K_d values were found to be 1.89, 35, and 34 nM for OKT3, CD3 scFv, and BiAb with R^2 values of 0.99, 0.985, and 0.99, respectively. AU, arbitrary units.

pAbBD was derived from the hyperthermal variant of the protein G B1 domain (HTB1) and includes the photoreactive unnatural amino acid, benzoyl phenylalanine (BPA), at the A24 site (*20*). This substitution places BPA within close proximity of the CH2-CH3 hinge on the IgG heavy chain (Fc region) and enables efficient photocrosslinking to most species and subclasses of IgG upon exposure to nondamaging, long wavelength ultraviolet (UV) light (365 nm) (*19*). The exact conjugation site is likely at methionine 252, because its presence was previously found to correlate to the ability to photocrosslink antibodies of various species (*19*). Two different anti-CD3–targeting domains were evaluated, a single-chain variable fragment (scFv) derived from the antibody OKT3 (*21*) and a CD3-targeted nanobody (*22*).

BiAbs were prepared by mixing the pAbBD–anti-CD3 fusion proteins with the desired antibody and then irradiating with 365-nm light for 2 hours. Six different T cell–redirecting BiAbs were created simultaneously from three Food and Drug Administration (FDA)–approved IgG1 antibodies—cetuximab [anti–epidermal growth factor receptor (EGFR)], rituximab (anti-CD20), and trastuzumab (anti-HER2)—and three additional human IgG subclasses—IgG2, IgG3, and IgG4 (Fig. 1B and fig. S1A). The photocrosslinking is nearly 100%, resulting in BiAbs with two pAbBD–anti-CD3 per IgG (one pAbBD–anti-CD3 per heavy chain). Nonreducing SDS–polyacrylamide gel electrophoresis (SDS-PAGE) and fast liquid protein chromatography traces of cetuximab before and after photocrosslinking further confirm nearly 100% conversion, and no higher or lower molecular weight side products were detected (fig. S2). This approach can be further parallelized to create hundreds or even thousands of BiAbs simultaneously, for possible screening applications. As proof of principle,

we generated 80 BiAbs in a single photocrosslinking experiment with each reaction ranging 92 through 98% heavy-chain conversion efficiency (fig. S3). The resulting tetravalent BiAbs are easily separated from free excess pAbBD–anti-CD3, which are much smaller in size, by ultrafiltration spin columns or dialysis, yielding a final BiAb with a purity greater than 95% and yield greater than 90%.

A notable feature of using pAbBD–anti-CD3 fusion proteins to generate BiAbs is the short production time compared with existing genetic methods. Following cloning and transformation, the pAbBD–anti-CD3 fusion proteins are expressed and purified in less than 3 days. BiAb photocrosslinking requires just 2 hours, and removal of excess fusion protein can be completed on the same day. Therefore, the overall procedure requires just 4 days from start to finish and just a single day if pAbBD–anti-CD3 fusion proteins have already been prepared. In comparison, the timeline for creating a new hybridoma and producing a BiAb is on the order of months.

Evaluation of photocrosslinked BiAb binding and T cell activation

To demonstrate that the photocrosslinking of pAbBD–anti-CD3 onto fusion proteins to IgG does not negatively affect antigen binding, we compared the relative affinity of BiAbs against the FDA-approved monospecific, monoclonal antibodies from which they were derived. The relative binding affinity was assessed by incubating the monospecific antibodies and the BiAb with corresponding HER2$^+$, EGFR$^+$, or CD20$^+$ adherent cell lines. Dose-dependent binding was detected using fluorescent secondary antibodies (Fig. 1, C to E, and fig. S1B). Our results indicate that there is no statistically significant

difference in the relative binding affinity between the BiAbs and the corresponding unconjugated, monospecific antibodies. These results confirm that the site-specific, covalent attachment of the pAbBD–anti-CD3 to IgG does not interfere with antigen binding.

Binding of the BiAbs to CD3 T cells was also assessed by comparing its relative affinity to the full-length anti-CD3 antibody (OKT3) and free anti-CD3 scFv. The relative binding affinity of BiAbs for CD3 was found to be similar to free anti-CD3 scFv (Fig. 1F). The different binding affinities observed in the OKT3 positive control versus the free and cross-linked anti-CD3 scFv could be due to the different detection methods used. OKT3 was indirectly detected with a fluorescent secondary, while the free scFv and the BiAb were directly detected as the scFv and pAbBD-scFv were labeled with one fluorophore using sortase-tag expressed protein ligation (STEPL) and GGG-TAMRA (5-carboxytetramethylrhodamine) (23). Nonetheless, the BiAbs can activate human T cells and trigger interferon-γ production in a dose-dependent manner, similar to full-length OKT3 (fig. S4).

T cell–mediated cytolysis with photocrosslinked BiAbs

The therapeutic potential of the photocrosslinked BiAbs was evaluated via in vitro T cell–mediated cytolysis. Specifically, anti-HER2 (trastuzumab) × anti-CD3, anti-EGFR (cetuximab) × anti-CD3, and anti-CD20 (rituximab) × anti-CD3 BiAbs were incubated with the respective HER2^{+}, EGFR^{+}, or CD20^{+} cell lines. T cells were added at an effector-to-target (E:T) ratio of 10:1, and cell lysis was monitored using xCELLigence real-time cell analysis (RTCA) for 72 hours (Fig. 2, A to C, and fig. S5). The BiAbs all exhibited dose-dependent cytotoxicity, with efficacies that are similar to what was previously reported

for alternative genetically engineered BiAb formats (24–26), although direct comparisons must be made with caution due to the variability among cell lines and T cell donors (26). Notably, cytolysis was not observed when nontargeted BiAbs or mixtures of unconjugated monoclonal antibody and anti-CD3 targeting domains were used. The kinetics of cell killing was rapid, increasing immediately after the addition of the BiAb and plateauing within 12 hours (Fig. 2, D and E, and figs. S6 and S7A). The therapeutic potential of the photocrosslinked BiAbs was evaluated via in vitro T cell–mediated cytolysis. Specifically, anti-HER2 (trastuzumab) × anti-CD3, anti-EGFR (cetuximab) × anti-CD3, and anti-CD20 (rituximab) × anti-CD3 BiAbs were incubated with the respective HER2^{+}, EGFR^{+}, or CD20^{+} cell lines. T cells were added at an E:T ratio of 10:1, and cell lysis was monitored using xCELLigence RTCA for 72 hours (Fig. 2, A to C, and fig. S4). The BiAbs all exhibited dose-dependent cytotoxicity, with efficacies that are similar to what was previously reported for alternative genetically engineered BiAb formats (24–26), although direct comparisons must be made with caution due to the variability among cell lines and T cell donors (26). Notably, cytolysis was not observed when nontargeted BiAbs or mixtures of unconjugated monoclonal antibody and anti-CD3 targeting domains were used. The kinetics of cell killing was rapid, increasing immediately after the addition of the BiAb and plateauing within 12 hours (Fig. 2, D and E, and fig. S5 and S6A).

Cytolysis of EGFR^{+} cells was also measured as a function of increasing E:T ratio using the anti-EGFR × anti-CD3 BiAb at a dosage of 0.1 or 1 nM (Fig. 2F and fig. S7B). Cytolysis was observed with an E:T ratio as low as 1:1, albeit low (<10%), and plateaued at an E:T ratio of 10:1. Mixtures of unconjugated monoclonal antibodies and
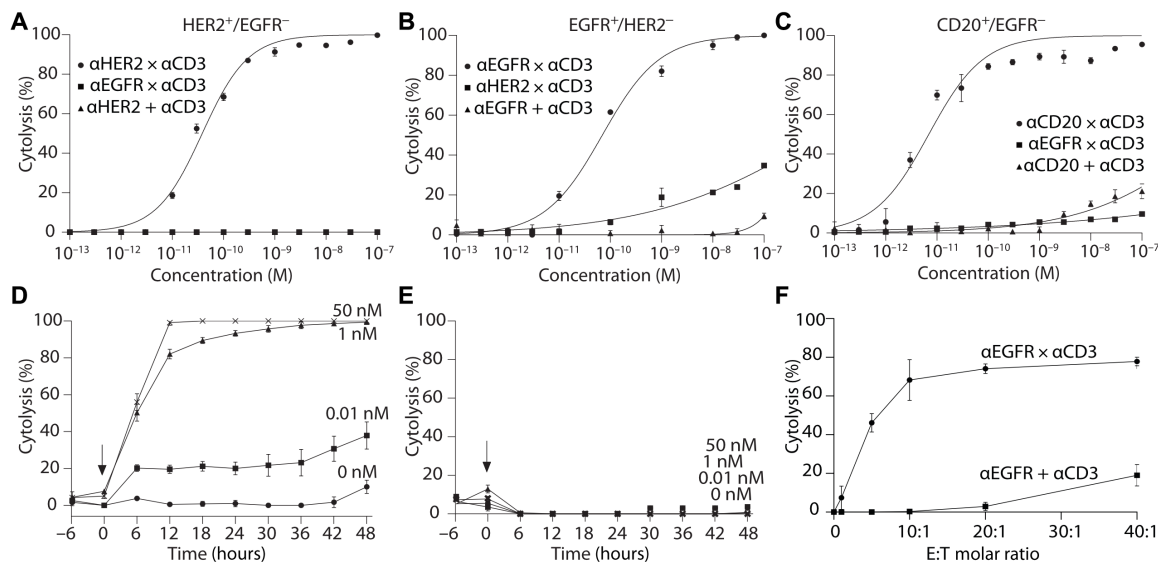

Fig. 2. BiAb functionality is confirmed by the T cell–mediated in vitro cytolysis targeted against HER2, EGFR, and CD20. (**A** to **C**) T cell–mediated cytolysis of HER2^{+} T617, EGFR^{+} MDA-MB-468, and CD20^{+} HT1080 cell lines was monitored for 72 hours as a function of BiAb dose using an xCELLigence real-time cell analysis (RTCA) instrument. Increasing concentrations of anti-HER2 (trastuzumab) × anti-CD3, anti-EGFR (cetuximab) × anti-CD3, and anti-CD20 (rituximab) × anti-CD3 BiAbs were analyzed (circles), as well as mixtures of the respective unconjugated antibodies and anti-CD3 scFv (triangles), and nontargeted BiAbs (squares). The nontargeted BiAbs in (A) and (C) consisted of an anti-EGFR × anti-CD3 BiAb and were tested on EGFR-negative cell lines (HER2^{+}/EGFR^{−} and CD20^{+}/EGFR^{−}, respectively), while in (B), an anti-Her2 × anti-CD3 BiAb was tested on an EGFR^{+}/HER2^{−} cell line. Here, BiAbs were prepared using the pAbBD–anti-CD3 scFv. Equivalent studies using the nanobody format are presented in fig. S4. All assays were performed with human T cells at a 10:1 E:T ratio. BiAbs EC$_{50}$ values were (A) 0.038 nM, (B) 0.05 nM, and (C) 0.007 nM. All R^2 values were greater than 0.9. (**D** and **E**) Kinetics of T cell–mediated cytolysis of EGFR^{+} tumor cells for (D) increasing concentrations of anti-EGFR (cetuximab) × anti-CD3 BiAb or (E) a mixture of anti-EGFR cetuximab and anti-CD3 scFv. All assays were performed with human T cells using an E:T of 10:1. (**F**) T cell–mediated cytolysis of EGFR^{+} cells with increasing E:T ratios, 12 hours after treatment with 0.1 nM EGFR-targeted BiAbs produced with pAbBD–anti-CD3 scFv or 0.1 nM cetuximab mixed with 0.2 nM free anti-CD3 scFv.

anti-CD3–targeting domains only showed appreciable killing (~20%) when the E:T ratio was increased to 40:1. Similar cytolysis trends were observed with both the anti-CD3 scFv and the anti-CD3 nanobody. Last, we also compared in vitro cytolysis using human T cells from three different donors in parallel and found minimum differences in the dose-dependent curves against EGFR$^+$ cells at an E:T ratio of 10:1 (fig. S7C).

T cell–redirecting autoantibodies

The unique ability to create highly uniform BiAbs via the site-specific, chemical modification of native antibodies with pAbBD–anti-CD3 led us to explore the feasibility of a therapeutic paradigm that cannot be achieved with genetic engineering approaches. Specifically, autoantibodies were isolated from tumor bearing mice and were converted into TRAAbs by photocrosslinking with pAbBD–anti-CD3, before being introduced back into mice as a form of personalized cancer therapy (Fig. 3A). The use of autoantibodies takes advantage of the immune system's innate ability to detect tumor-specific targets and circumvents the need to identify tumor antigens. Moreover, because TRAAbs are derived from a pool of IgGs that can recognize diverse tumor targets, they have the potential to overcome many of the shortcomings that plague monoclonal antibody therapy, such as heterogeneity in target expression within tumors, patient-to-patient variability, and antigen down-regulation.

The potential for TRAAb therapy was initially established using two different cancer human cell lines, Nalm-6 leukemia cells and MDA-MB-468 breast carcinoma cells. Autoantibodies were raised against these tumor cells via repeated intraperitoneal administration into immunocompetent C57BL/6J mice (Fig. 3B). Blood was collected, and all IgGs, including tumor-specific autoantibodies, were isolated 2, 4, and/or 8 weeks after the first administration of cancer cells. Tumor-specific autoantibodies extracted after 8 weeks of Nalm-6 exposure were found to bind Nalm-6 tumor cells with a 4.1×10^{-8} M affinity. Control wild-type (WT) IgGs from healthy mice did not
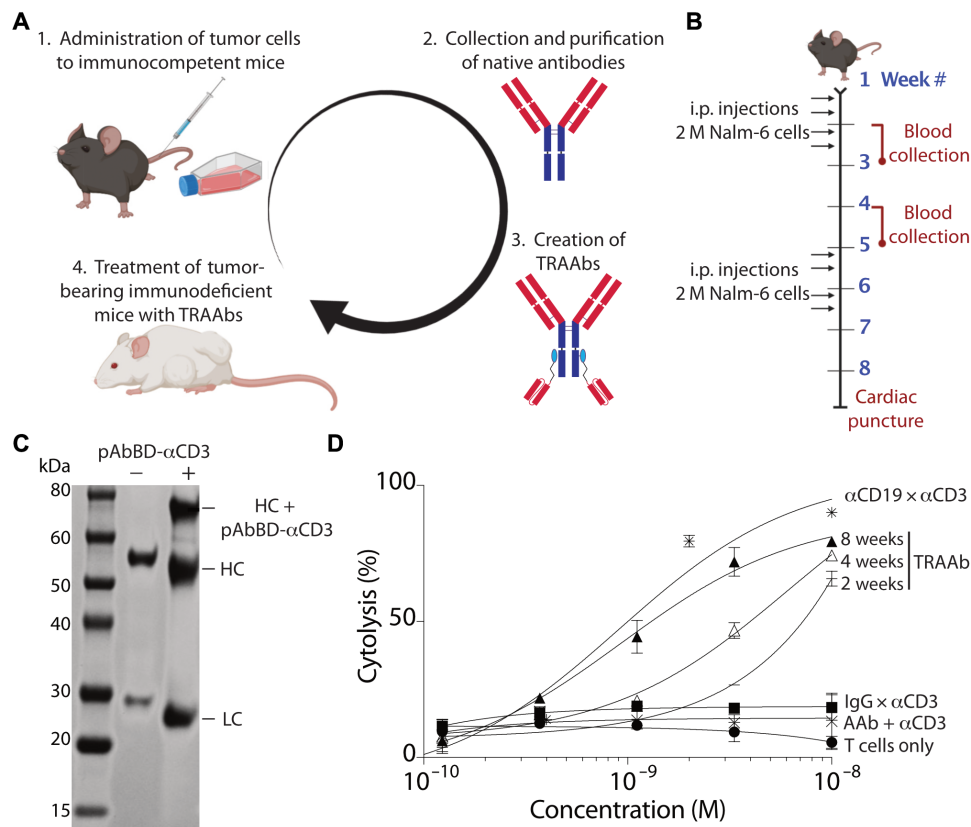

Fig. 3. pAbBD-mediated production of TRAAbs creates personalized, functional targeted therapeutics without needing to identify tumor markers. (**A**) Endogenous extracted from the serum of mice vaccinated with Nalm-6 B cells were converted into TRAAbs via site-specific, covalent photocrosslinking of the pAbBD–anti-CD3 fusion protein. The tumor killing capability of the resulting BiAbs was evaluated in vitro and in vivo using immunodeficient mice engrafted with human T cells. (**B**) Whole-tumor vaccination of C57BL/6 immunocompetent mice with CD19$^+$ Nalm-6 B cell leukemia was completed as follows: 2×10^6 cells were intraperitoneally (i.p.) injected twice a week for 2 weeks, followed by 2 weeks off. This 28-day cycle was repeated twice before collecting the entire blood volume via cardiac puncture. Blood samples were also collected after the second and fourth weeks. (**C**) Blood samples of vaccinated mice were centrifuged to extract serum, and all IgGs, including tumor-specific autoantibodies (AAbs), were purified using protein G agarose resin. TRAAbs were produced via photocrosslinking with a pAbBD–anti-CD3 nanobody. Heavy chain (HC) and light chain (LC) are shown before and after photocrosslinking on a reducing SDS-PAGE. (**D**) Luciferase-expressing CD19$^+$ Nalm-6 B cell leukemia cells were incubated with human T cells, using a 5:1 E:T, and cytolysis was analyzed using the Steady-Glo Luciferase Assay System (Promega) 24 hours after antibody treatment. Treatments included BiAbs that were generated by photocrosslinking pAbBD–anti-CD3 nanobodies to (i) AAbs extracted from vaccinated C57BL/6 mice (i.e., TRAAbs), (ii) IgGs extracted from WT C57BL/6 mice, and (iii) control anti-CD19 IgGs (MAB1794, EMD Millipore). A T cell only control was also tested. The EC$_{50}$ values were found to be 0.92 nM for TRAAbs, using AAbs that were collected 8 weeks after the first Nalm-6 injection ($R^2 = 0.99$), and 0.90 nM for the anti-CD19 × anti-CD3–positive control ($R^2 = 0.95$).

bind Nalm-6 cells at the concentrations tested. The pool of IgGs including autoantibodies was then converted to TRAAbs and evaluated in T cell–mediated cytolysis assays, using the same cells that were introduced into mice to generate an antitumor response. The efficiency of photocrosslinking between pAbBD–anti-CD3 and murine autoantibodies was ~50% (Fig. 3C), which is lower than the photocrosslinking efficiency to human IgG. This is likely due to the known low cross-linking efficiency between pAbBD and mIgG1 (*19*). Nonetheless, the TRAAbs led to the potent, dose-dependent cytolysis of both Nalm-6 (Fig. 3D) and MDA-MB-468 cells (fig. S9), using the respective TRAAbs. Nontargeted TRAAbs, generated from antibodies isolated from healthy mouse serum, and mixtures of the unconjugated autoantibodies and anti-CD3–targeting ligands did not result in any appreciable cytolysis at the doses tested. As expected, the therapeutic efficacy of the TRAAbs improved when autoantibodies were collected after more intraperitoneal administrations of the Nalm-6 cancer cells. TRAAbs produced from autoantibodies collected at 8 weeks following the first administration of CD19-positive Nalm-6 cells exhibited an EC_{50} (median effective concentration) of 0.92 nM, which is comparable to the 0.90 nM EC_{50} of a positive control consisting of an anti-CD19 × anti-CD3 BiAb.

Next, we tested whether TRAAbs could serve as an effective treatment for mice bearing Nalm-6 tumors. The Nalm-6 cells were engineered to express luciferase so that tumor growth could be monitored longitudinally by bioluminescent imaging. All TRAAbs for this study were produced using pAbBD–anti-CD3 nanobodies, due to their more reliable and higher expression, compared with pAbBD–anti-CD3 scFvs, which was necessary to facilitate the completion of this in vivo study. NSG mice were used in this study due to the need to use human T cells. A total dose of TRAAb (0.5 mg/kg), distributed across three intraperitoneal injections every other day, led to a statistically significant slowing of tumor progression and increased survival (100% over

60-day experiment), compared with untreated mice, mice treated with nontargeted TRAAbs, and mice treated with a mixture of unconjugated autoantibodies and anti-CD3 (Fig. 4 and fig. S10A). The mixture of unconjugated autoantibodies and anti-CD3 did lead to some slowing of tumor growth and improvement in median survival compared with the other controls, but the statistically significant difference between this control and the TRAAbs demonstrates the benefit of a physical link between the autoantibodies and the anti-CD3–targeting domain. The intraperitoneal injection of TRAAbs into the mice led to no signs of illness, change in activity, or weight loss (fig. S10B).

In a second study, a total dose of TRAAb (2.5 mg/kg) was intraperitoneally administered over the course of five consecutive days into mice 4 days after injection of Nalm-6 tumor cells, corresponding to a more advanced stage of disease (fig. S10C). The tumors initially regressed, compared with untreated mice and mice treated with nontargeted TRAAbs, but this was followed by tumor recurrence. Nonetheless, there was a notable and statistically significant slowing of tumor growth and reduction in tumor burden after treatment, compared with all controls.

Syngeneic TRAAbs: Tumor-specific binding and in vitro cytolysis

After demonstrating that autoantibodies raised against human tumor cell lines in mice could be converted into TRAAbs and elicit a potent cytolytic effect, we next tested whether TRAAbs generated from endogenous, circulating antibodies in a syngeneic murine cancer model (Fig. 5A) could also produce similar cytolytic effects. First, we tested the binding affinity of IgGs extracted from the serum of mice growing CT26 colorectal tumors, 4T1 triple-negative breast tumors, and RENCA renal cortical tumors (Fig. 5B and fig. S11). In all three models, a therapeutic window was observed between the IgGs extracted
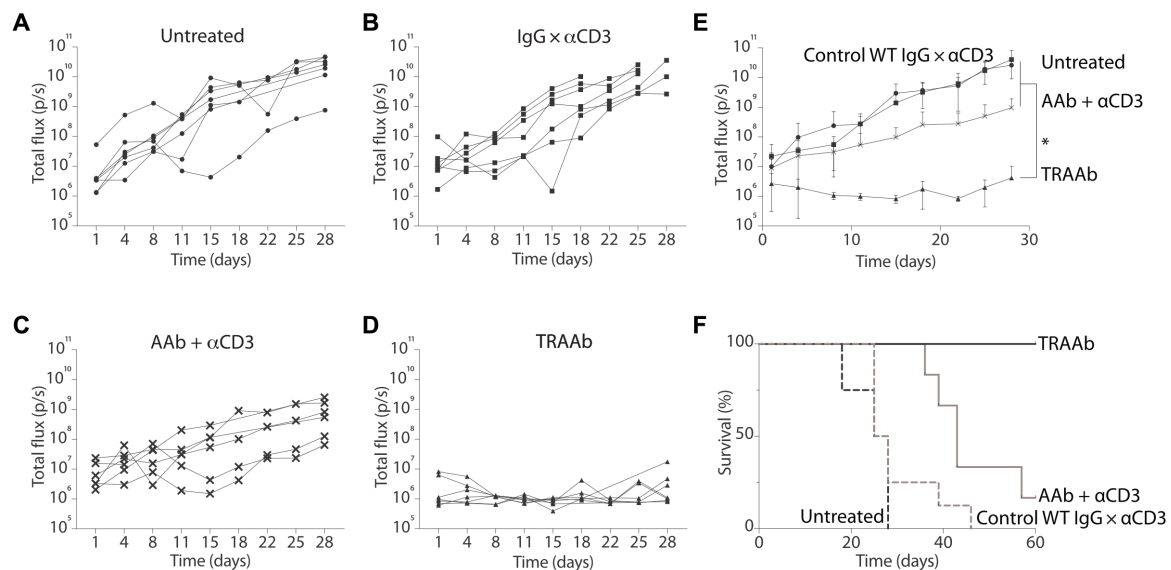

Fig. 4. TRAAb therapeutic efficacy is confirmed by in vivo tumor suppression and improved survival. (**A** to **D**) Immunodeficient NSG mice were injected with 0.5 M Nalm-6 B cell leukemia cells and (A) left untreated, or treated with 10 M human T cells and a total dose of 0.5 mg/kg of (B) BiAbs produced from IgGs extracted from WT nonvaccinated mice, (C) mixed AAbs and anti-CD3 nanobody, or (D) TRAAbs. Treatment was evenly distributed along days 1, 3, and 5, as was 1 mg of background, WT polyclonal murine IgG (BE0093, Bio X Cell). Tumor growth was tracked twice per week via luciferase expression and D-luciferin (PerkinElmer) injections using the IVIS Ilumina system. (C and D) p/s photons/s. (**E**) Averaged bioluminescence readings for groups depicted in (A) to (D). n = 6 or 7. At day 28, *P < 0.05 or smaller between TRAAb and all controls. (**F**) Sixty-day survival Kaplan-Meier curves.
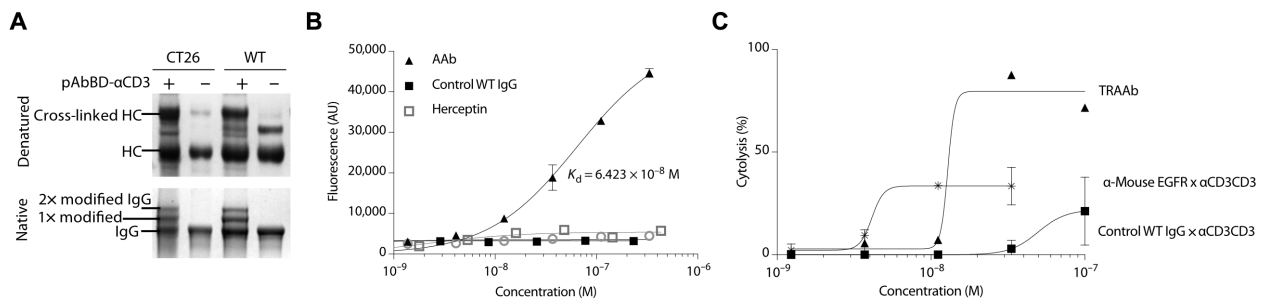
Fig. 5. Functionality of TRAAbs produced using syngeneic, endogenous antibodies. (**A**) Endogenous antibodies were extracted from the sera of BALB/c mice growing syngeneic CT26 colorectal tumors subcutaneously, as well as WT BALB/c mice. The purified IgG were photocrosslinked with pAbBD–anti-CD3, to create TRAAbs, and run on a denaturing and native SDS-PAGE. (**B**) Endogenous IgGs from mice with CT26 tumors (AAbs) bind CT26 cells specifically, while no significant binding was observed with control WT IgGs from healthy BALB/c mice and nontargeted anti-human HER2 (Herceptin). (**C**) TRAAbs produced using IgGs from CT26 tumor–bearing mice yielded dose-dependent tumor cytolysis 24 hours after treatment, as does a positive control targeted against mouse EGFR. A negative control composed of T cell recruiting WT IgGs led to minimal cytolysis and only at the highest concentration tested. All syngeneic in vitro studies were completed using an E:T ratio of 8:1.

from tumor-bearing mice versus control IgGs from healthy mice. The dissociation constant (K_d) values of the circulating IgGs were found to be 6.4×10^{-8}, 2×10^{-8}, and 1.3×10^{-8} M in the CT26, 4T1, and RENCA models, respectively.

The functionality of the syngeneic TRAAbs was assessed via T cell–mediated cytolysis of CT26 and 4T1 cells with the corresponding TRAAbs (Fig. 5C and fig. S12). Again, dose-dependent cytolysis with TRAAbs was observed using an E:T ratio of 8:1 in both models, while the nontargeted control BiAb composed of WT BALB/c IgGs photocrosslinked with pAbBD–anti-CD3 resulted in minimal cytolysis. The cytolysis results presented for syngeneic TRAAbs are representative of about half of the experiments performed. In the other half of the experiments, neither the TRAAbs nor the positive control yielded any cytolysis and thus were excluded from the analysis. This is notable because this high level of variability was not observed in prior studies; however, we believe that it most likely stems from differences in the activity of the freshly extracted T cells being used in each time.

Although the binding affinities of the autoantibodies extracted from the syngeneic models were relatively similar to the Nalm-6 autoantibodies, the syngeneic in vitro potencies were found to be lower. This could be due to the percent of tumor-binding autoantibodies within the whole pool of collected IgGs differing. In addition, the Nalm-6 suspension cells might be inherently more sensitive to T cell–mediated cytolysis in comparison to the syngeneic models used here, which are all solid tumors (renal and breast). Overall, these findings further demonstrate the cytolytic potential of TRAAbs collected from two syngeneic models, one of which has no preidentified druggable targets.

Binding of endogenous antibodies to tumors versus healthy tissues in syngeneic models

To further explore the therapeutic window of TRAAbs, we evaluated their ability to distinguish tumor versus healthy tissue. To assess whether endogenous, circulating antibodies preferentially bind to tumor tissue, the tumor, heart, liver, spleen, kidney, and lungs of BALB/c mice bearing 4T1 and CT26 tumors were harvested and stained with endogenous IgG (Fig. 6, A, C, D, and E). In both models, the signal detected in the tumor was significantly higher than that of the healthy tissues, indicating a therapeutic window. Our results in the 4T1 model match the trend previously reported (27). To further confirm our results, the CT26-HER cell line was also used, and the signal using a murine

anti-human HER2/neu-positive control was found to be significantly higher in the tumor versus all the other healthy tissues lacking human HER2/neu (Fig. 6B). While these results do not entirely eliminate the possibility of T cell redirection toward healthy tissues against which autoantibodies might be produced, they indicate a possible therapeutic window for safe therapy.

Preparation of TRAAbs from human antibodies

While many hurdles would need to be overcome before TRAAbs could be considered for human therapeutic use, we believe that the approach is conceptually feasible. As an initial demonstration of feasibility, TRAAbs were produced using IgGs derived from the serum of two patients with liver cancer. The cross-linking efficiency of the pAbBD–anti-CD3 fusion protein to the heavy chains was ~75% (fig. S13, A and B). The IgG extraction yield averaged around 1.4 mg/ml of blood. For context, the IgG extraction yield averaged 0.31, 0.49, and 1.54 mg/ml of blood for mice bearing 4T1, CT26, and Nalm-6 tumors, respectively (fig. S13, C and D).

Following clinical standards that allow 2.5% blood volume to be drawn at once would allow collection of ~150 ml of blood for a patient weighing 75 kg, yielding at least 210 mg of IgG. This would allow for a maximum achievable dose of 2.8 mg of TRAAbs per kilogram, which surpasses the doses used in this manuscript (0.5 and 2.5 mg/kg). The concentration of circulating IgGs in human serum is around 10 mg/ml; with further development of the IgG extraction protocol, the maximum achievable dose could increase by another factor of 10.

DISCUSSION

This work outlines and validates a rapid and efficient method for producing BiAbs via the site-specific modification of "off-the-shelf" and endogenous serum autoantibodies with T cell–redirecting domains. IgGs are covalently labeled in a site-specific manner using pAbBDs. pAbBDs are derived from the HTB1 domain of the naturally occurring bacterial protein G (18), which binds to the IgG Fc region with nanomolar affinity (19), resulting in a maximum of two pAbBDs cross-linked onto each IgG. Once bound, UV exposure drives covalent cross-linking via the incorporated unnatural amino acid BPA within the pAbBD. The entire process requires just two steps, mix and illuminate, and is completed in just 2 hours. Subsequent
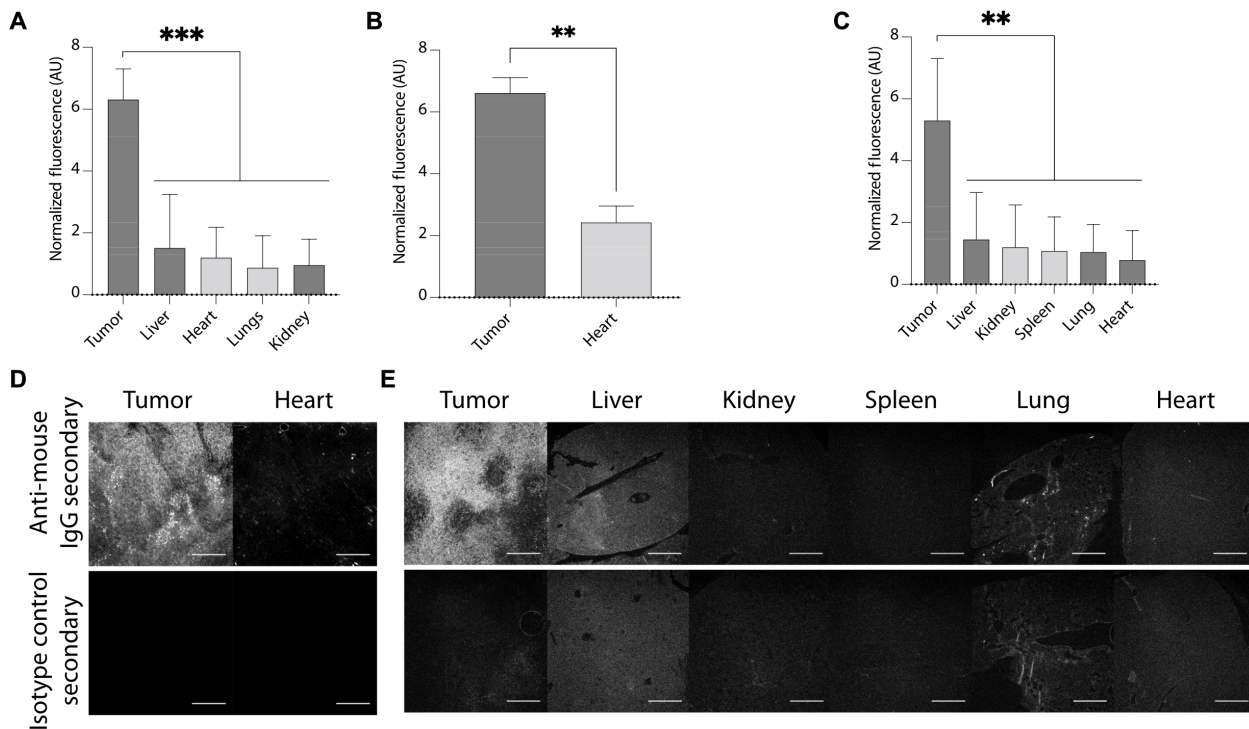
Fig. 6. Circulating endogenous antibodies preferentially target tumor tissue over healthy tissues in two syngeneic models. (**A**) Immunofluorescent staining of syngeneic colorectal CT26 tumor tissue and healthy tissue of major organs where endogenous antibodies isolated from CT26 tumor–bearing mice were used as the primary antibody. The fluorescent signal was quantified and normalized to controls using isotype control secondary antibodies, $n = 5$, $P < 0.001$ or smaller. (**B**) Replicate of (A) using positive control cell line CT26-HER2 that was engineered to express human HER2/neu receptor. Here, staining was done using murine anti-human HER2/neu as a primary antibody. $n = 3$, $P < 0.01$. (**C**) replicates of (A) in triple-negative breast cancer 4T1 model. $n = 5$, $P < 0.01$. (**D** and **E**) Representative images used for above quantifications of CT26 and 4T1 circulating antibodies bound on tumor tissues versus healthy tissues of major organs. Scale bar represents 500 microns.

purification by ultrafiltration or dialysis can result in >95% purity and >90% yield, owing to the high photocrosslinking efficiency and the large size difference between the BiAb and the pAbBD–anti-CD3.

To demonstrate the versatility and robustness of this approach, six different T cell–recruiting BiAbs were produced in parallel by labeling three FDA-approved IgG1 antibodies (cetuximab, trastuzumab, and rituximab) and three human IgG subclasses (IgG2, IgG3, and IgG4) with an anti-CD3 targeting domain. Two different anti-CD3 targeting domains were tested, an scFv derived from the antibody OKT3 and a nanobody. The resulting BiAbs were able to bind both the tumor antigen and the CD3 receptor with the same affinities as the individual components and induce targeted in vitro tumor cytolysis in a dose-dependent manner. Together, the binding affinity and the T cell–mediated cytolysis results show that pAbBD-mediated BiAb production yields functional therapeutic constructs.

The pAbBD can label nearly all IgGs, including IgGs from diverse species and their subclasses (*19*, *28*, *29*), suggesting that its use in BiAb production can be applied to virtually any candidate antibody of interest. Moreover, cross-linking is highly reproducible and can be parallelized, which was demonstrated with the simultaneous photocrosslinking of 80 IgGs with pAbBD–anti-CD3 in parallel, with nearly 100% conversion efficiency for every sample. Bispecific production can likely be further scaled up to assess hundreds or thousands of antibodies at once using multiple 96-well plates. This higher throughput BiAb production could be valuable in validating targets and identifying favorable epitopes and/or synergistic binding partners. Of course, to realize the full potential of this capability,

future work needs to investigate whether BiAbs produced with pAbBDs can accurately predict the relative efficacy of alternative BiAb formats that are more favorable for clinical translation. While it has previously been shown that different BiAb formats can display large differences in efficacy (*30*), it is not clear whether the correlation between efficacy and specific antibody pairs is maintained across diverse platforms. Nonetheless, it should be noted that the BiAb presented here is highly similar in structure to BiAbs with scFvs fused to the C terminus of the heavy chain (e.g., Sanofi/SAR156597, Merrimack/MM141, and Aptevo/Mor209/ES414) and thus is more likely to be predictive of at least this platform.

Perhaps the most valuable attribute of using pAbBDs to create BiAbs is the ability to rapidly explore unique and complex therapeutic constructs. For example, the anti-CD3 binding portion can be replaced with other protein cargos, such as alternative cellular recruiting elements, e.g., for natural killer cells (*31*), or tested in combination with chemical moieties, such as drugs or imaging agents (*32*). Chemical moieties can easily be attached to the pAbBD–anti-CD3 (or other fusion construct), via enzyme mediated ligation (*33*). In addition, multiple targeting domains can be fused to pAbBDs in tandem, either against the same target or different targets, to create higher affinity or multispecific constructs. Engineering of pAbBDs is simple, compared with full-length antibody and antibody fragment fusion proteins, due to the pAbBD's small size, highly stable structure, lack of disulfides, and high expression levels as soluble proteins in *Escherichia coli*.

To highlight how pAbBDs can be used to explore unique therapeutic approaches that cannot be pursued with conventional genetically

engineered BiAbs, we generated T cell–redirecting autoantibodies (TRAAbs). Here, we were interested in testing whether endogenous, circulating antibodies could be used as the targeting unit in T cell–redirecting BiAbs. The unique specificity of endogenous, tumor-associated autoantibodies that are found in circulation in the serum of patients with cancer has led them to be widely evaluated as bio-markers, prognostic factors, and indicators of tumor recurrence (27, 34–45). By converting autoantibodies into TRAAbs, we harnessed this unique specificity while also taking advantage of the potent therapeutic effect provided by T cell recruitment. Here, autoantibodies extracted from the serum of mice vaccinated with human B cell leukemia cells were labeled with pAbBD–anti-CD3. TRAAb functionality was demonstrated via dose-dependent cytolysis of four different cancer cell lines in vitro and tumor regression and improved survival in vivo. Two of the tumor models used to generate TRAAbs were syngeneic, one of them being a triple-negative breast cancer model for which there are now no clinically validated targets. Furthermore, the extracted endogenous IgGs of both syngeneic models were found to preferentially bind tumor tissue versus healthy tissue of major organs, indicating an appreciable therapeutic window.

Many questions still need to be answered before TRAAbs can be considered for clinical use. First, the potency of the humoral response as a function of time would need to be further elucidated. In the Nalm-6 studies, we found that the potency of TRAAbs increased with the number of immunizations. The relationship between humoral response and clinical stage requires further investigation and is likely to dictate how and when TRAAbs can be offered as a therapeutic option. Second, the pAbBDs used here are bacterial in origin, which could limit their clinical utility. However, it should be noted that therapeutic proteins derived from other bacterial antibody-binding domains have already been tested in multiple different clinical trials and have been fund found to be safe (46–49). Alternatively, it is conceivable that analogous pAbBDs could be derived from human proteins that exhibit a high affinity for IgG (50, 51). Third, because pAbBDs bind to the same region of IgG as the neonatal Fc receptor (FcRn), it could negatively affect the circulation half-life of TRAAbs. One possible solution may be to use a 1:1 pAbBD-to-IgG molar ratio, which would free up one Fc site for FcRn binding. Fourth, although TRAAbs are likely to have a therapeutic window, it is well known that endogenous autoantibodies can also bind healthy tissues and therefore may still elicit an off-target effect (52–54). Further studies are required to assess such dose-dependent toxicities. One possible approach to alleviate these concerns would be to identify a method that could allow for the separation of antitumor antibodies from other endogenous antibodies. Last, the production method presented here uses UV photocrosslinking to drive the formation of BiAbs. The question of how this would scale up remains open ended, as with any new manufacturing method. Despite these unknowns, we believe that TRAAbs represent an unexplored paradigm in cancer immunotherapy. Our data point to the possibility of a cellular recruiting treatment that can circumvent antigen identification and overcome patient-to-patient variability and tumor heterogeneity. Furthermore, by targeting a broad pool of tumor antigens, TRAAb therapy could remove the selection pressure that is associated with targeted immuno-therapies and is believed to drive antigen loss and tumor recurrence. In summary, we believe that pAbBD-mediated BiAb production will serve as a robust tool for research and development of new antibody-based immunotherapies, including personalized strategies that use the immune system's innate ability to recognize tumor targets.

MATERIALS AND METHODS
Cloning
To prepare BiAbs, a pAbBD with BPA introduced at the A24 site (19) was fused with an anti-CD3 scFv derived from full-length OKT3 antibody (21) or with an anti-CD3 nanobody (22). For the pAbBD–anti-CD3 scFv fusion protein, the DNA coding sequences were inserted into a Nde I– and Xho I–digested proximity-based sortase-mediated ligation (PBSL) vector (33). For the pAbBD–anti-CD3 nanobody fusion protein, the DNA coding sequence was first cloned in-frame with our STEPL expression system (23) and then inserted into a Nde I– and Bam HI–digested pmjs187 vector, which was provided by L. Ruddock (University of Oulu). A second plasmid was cloned to include an additional copy of the anti-CD3 nanobody in addition to pAbBD–anti-CD3 nanobody. For both scFv and nanobody formats, a control construct was also cloned without pAbBD.

All synthesized DNA sequences were codon-optimized for *E. coli* expression and produced by Integrated DNA Technologies. Synthesized DNA sequences were inserted into vectors that were double-digested with the aforementioned restriction enzymes and cloned using In-Fusion HD Cloning (Clontech). Cloning was verified by Sanger sequencing. Protein and DNA sequences for all purified proteins are listed in table S1.

Protein expression and characterization
Origami B(DE3) Competent Cells (EMD Millipore) were cotrans-formed with the pAbBD–anti-CD3 scFv plasmid and the pEVOL-pBpF plasmid (Addgene, plasmid no. 31190), which carries the transfer RNA/aminoacyl transferase pair (20). T7 Express Competent Cells (Invitrogen) were cotransformed with pEVOL-pBpF and the pAbBD–anti-CD3 nanobody fusion as well as the version containing a second copy of the anti-CD3 nanobody. The anti-CD3 scFv and nanobody without pAbBD were also transformed into T7 Express and Origami B(DE3), respectively.

Bacterial starter cultures were grown overnight at 37°C in a shaker in 2 ml of LB + ampicillin (100 µg/ml) + chloramphenicol (25 µg/ml). Starter cultures were added at a 1:1000 dilution to Autoinduction Media LB Broth Base Including Trace Elements (Formedium) with ampicillin (100 µg/ml) and chloramphenicol (25 µg/ml). For BPA incorporation, L-benzoylphenylalanine (Bachem, King of Prussia, PA) was added into the medium to a final concentration of 500 µM, and arabinose was added to a final concentration of 0.1% to induce the pEVOL promoter. The pAbBD–anti-CD3 scFv and the free scFv were expressed in a 25°C shaker for 72 hours, while the pAbBD–anti-CD3 nanobody and the free nanobody were expressed in a 37°C shaker for 24 hours. The pAbBD–anti-CD3-anti-CD3 version containing two nanobodies was expressed at 25°C for 8 hours.

After bacterial recombinant expression of the pAbBD–anti-CD3 proteins, cultures were pelleted by centrifugation (5500g for 15 min at 4°C) and purified as previously described (23, 33). SDS-PAGE electrophoresis was performed on Bolt 4 to 12% Bis-Tris Plus Gels (Thermo Fisher Scientific) with a Mini Gel Tank (Thermo Fisher Scientific), stained with SimplyBlue SafeStain (Invitrogen), and imaged using a Gel Logic 100 system (Kodak).

Photocrosslinking of pAbBD-CD3 fusion proteins onto IgGs
To create T cell–redirecting BiAbs and TRAAbs, the purified recombinant pAbBD-CD3 fusion proteins were mixed with the IgG of choice (cetuximab, rituximab, trastuzumab, or endogenous antibodies) using a slight excess of at least 2.5:1 molar ratio and exposed

to long wavelength UV light (365 nm) for 2 hours (19). The photo-crosslinked IgGs were purified by removing excess pAbBD–anti-CD3 using 100-kDa molecular weight cutoff (MWCO) filters (Amicon Ultra, Milipore, Temecula, CA) or dialyzing into sterile phosphate-buffered saline (PBS) using a cellulose ester membrane (Spectra/Por). Final sample concentrations were assessed by reducing SDS-PAGE comparing against known amounts of IgG. Conversion efficiency of the heavy chains was estimated via gel band intensity using ImageJ.

To further characterize the photocrosslinking reaction, fast protein liquid chromatography was performed using an Akta Pure and a Superdex 200 Increase 10/300 GL size exclusion column. The flow rate used was 0.5 ml/min, and the standards used were the Bio-Rad gel filtration standards (catalog no. 1511901).

Binding affinity assays

The relative binding affinity of BiAbs versus the corresponding unconjugated monoclonal antibodies were assessed using HER$^+$ T617 cells (provided by M. Greene, University of Pennsylvania), CD20$^+$ HT1080 cells (transduced with human CD20 Full-length containing lentivector from G&P Bioscience), and EGFR$^+$ MDA-MB-468 [American Type Culture Collection (ATCC)] cells. The binding affinities of syngeneic TRAAbs were evaluated using 4T1 (ATCC) as well as CT26 and CT26-HER cell lines, provided by C. Simon and M. Greene, respectively.

Cells were seeded on clear-bottom, black-walled 96-well plates in 100 µl of Dulbecco's modified Eagle's medium (DMEM) or RPMI culture medium [supplemented with 1% penicillin/streptomycin and 10% fetal bovine serum (FBS)] and kept in a 37°C cell culture incubator until at least 80% confluency was reached. The cells were fixed by 15-min incubation with 50 µl of 4% paraformaldehyde per well. After washing twice with 200 µl of PBST buffer (PBS, 0.05% Tween 20, pH-adjusted at 7.2), the cells were blocked with PBST with 4% normal donkey or goat serum for 1 hour. Serial dilutions of BiAbs or monoclonal antibodies were added to the target fixed cells and incubated at room temperature for 1 hour. After washing with PBST, cells were incubated for 1 hour with Rhodamine Red-X–conjugated donkey anti-human IgG (7.5 µg/ml; Jackson Laboratory) or phycoerythrin-conjugated goat anti-human or anti-mouse IgG (Invitrogen). Fluorescence readings were completed with an Infinity M200 (Tecan) or Synergy H1 (BioTek) plate reader. Binding curves were fit using a saturation (one-site–specific) binding model and K_d values were calculated using GraphPad Prism software (GraphPad Software, La Jolla, CA, USA).

The binding capabilities of BiAbs, OKT3, and free anti-CD3 scFv were analyzed using CD3$^+$ human T cells. EZ-Link Sulfo-NHS-LC-Biotin (Thermo Fisher Scientific) was used for labeling the antibodies. Serial dilutions of cells were incubated in FACS (fluorescence-activated cell sorting) buffer (PBS, 2% FBS) for 1 hour at 4°C. The cells were washed once with FACS buffer, resuspended to 1×10^6 cells/ml, and incubated with streptavidin-allophycocyanin (SA-APC) (BioLegend) 30 min at 4°C. After incubation with SA-APC, the cells were washed twice with FACS buffer and resuspended in 200 µl of FACS buffer. The fluorescence intensity of the stained cells was analyzed by flow cytometry.

Human T cells expansion

Healthy human T cells were obtained from the Human Immunology Core (University of Pennsylvania) and expanded as previously described (55). Briefly, equal amounts of CD4$^+$ and CD8$^+$ T cells were seeded and stimulated with anti-CD3/CD28 activator Dynabeads (Gibco) in a 1:1 ratio. Recombinant human interleukin 2 (Gibco) was added at 50 IU/ml on the following day and maintained at this concentration 10 days after seeding. The Dynabeads were magnetically removed 7 days after seeding. Cell density was maintained at 0.5 to 1 M/ml throughout the 14-day culture, and cell size distribution was tracked every other day to confirm activation and return to resting state. The final composition of CD4$^+$ versus CD8$^+$ T cells was checked at the end of the protocol and confirmed to be around ~60% CD8$^+$ and ~40% CD4$^+$. Following expansion, the expanded cells were frozen down using a 1:1 mixture of X-VIVO medium (Lonza) and 10% dimethyl sulfoxide (DMSO) FBS in aliquots (50 M/ml). The cells were thawed in DMEM cell culture medium 24 hours before using at a density of 5 M/ml.

Cytokine secretion assay

A 96-well plate was coated with 10 nM OKT3, BiAbs, or PBS buffer as a negative control overnight at 4°C. Twenty-four hours later, the wells were washed with PBS and T cells (1×10^6 cells per well) were added for overnight incubation at 37°C. Following the overnight incubation, the plate was centrifuged at 800g for 8 min. The supernatant was collected carefully without disturbing the cell pellet. The released interferon-γ in the supernatant was quantified using a commercial interferon-γ enzyme-linked immunosorbent assay kit (BioLegend).

T cell–mediated tumor cytolysis assays

For adherent EGFR$^+$, CD20$^+$, and HER2$^+$ target cells, in vitro T cell–mediated tumor cytolysis assays were performed with the corresponding target cancer cells in the presence of T cells either at a constant 10:1 E:T ratio with varying treatment concentrations or at constant treatment concentration and varying increasing E:T ratios, as indicated. Tumor cell viability was tracked using an xCelligence RTCA (ACEA Biosciences).

For suspension Nalm-6 cells, a constant 5:1 E:T ratio was maintained. Viability of Nalm-6 cells that were genetically engineered to express click beetle luciferase (provided by M. Milone, University of Pennsylvania) was tracked via luciferase bioluminescence. At each time point, 50 µl of room temperature Steady-Glo luciferin substrate (Promega) was thoroughly mixed with 50 µl of suspended cells. Bioluminescence was read using the Synergy H1 plate reader (Biotek). A CD19-CD3 BiAb-positive control was produced using MAB1794 (EMD Millipore) and included for comparison. Cytolysis curves were fit using a variable slope dose-response stimulation model, and EC$_{50}$ values were calculated using GraphPad Prism software (GraphPad Software, La Jolla, CA, USA).

Endogenous antibodies collection and binding characterization

All animal studies were conducted with approval by the University of Pennsylvania Institutional Animal Care and Use Committee, in accordance with the Association for Assessment and Accreditation of Laboratory Animal Care International guidelines and accreditation. Mice were fed standard chow ad libitum, unless otherwise noted. Autoantibodies were raised against either human EGFR$^+$ MDA-MB-468 breast cancer cells or human CD19$^+$ Nalm-6 B cell leukemia cells, engineered to express luciferase, by subjecting 6- to 10-week-old C57BL/6 mice (Charles River Laboratories, Wilmington, MA) to 2 weeks of biweekly intraperitoneal injections with 2×10^6 cells, followed by 2 weeks off. This 28-day cycle was repeated twice before collecting the entire

blood volume. The EGFR$^+$ MDA-MB-468 cells were treated with mitomycin C (40 μg/ml) before injecting the mice. In the Nalm-6 study, blood samples were also collected after the second and fourth week.

Syngeneic autoantibodies were collected from the sera of BALB/c mice 14 to 17 days after subcutaneously injecting 1×10^6 cells. Cells were separated from serum by 15-min high-speed centrifugation, and the antibodies were captured using recombinant protein G agarose resin (Invitrogen).

The binding affinity of autoantibodies collected from the sera of Nalm-6–exposed mice was assessed against live Nalm-6 cells. First, 1×10^5 Nalm-6 cells were incubated in 10% normal goat serum, washed in flow buffer (filtered PBS, 1% bovine serum albumin, and 1 mM EDTA), and further blocked using human FcR blocking solution (Miltenyi Biotec). Autoantibodies from Nalm-6–exposed and healthy mice were incubated 30 min at room temperature. After washing, a 30-min incubation at room temperature with 1:200 fluorescent secondary anti-mouse antibody (Invitrogen) was used to detect bound primary. Flow cytometry was performed with a BD Accuri C6.

Nalm-6 in vivo studies in NSG mice
TRAAbs preparation
pAbBD–anti-CD3 nanobodies and control proteins (pAbBD alone and the nanobody alone) were treated to remove endotoxin using 1% Triton X-114 phase separation (56). Following photocrosslinking to the isolated autoantibodies, TRAAbs were mixed with mouse polyclonal IgGs (BioXCell) to obtain 1 g of background, WT antibodies per mouse. These mixtures were dialyzed in sterile PBS using 100 MCWO cellulose membrane (Spectrum Labs) and concentrated using polymeric absorbent Spectra/Gel (Spectrum Labs).
Tumor model and treatment strategy
Male and female NSG mice, aged approximately 6 to 10 weeks, were obtained from Stem Cell Xenograft Core, University of Pennsylvania. A total of 5×10^5 Nalm-6 cells and 1×10^7 human T cells were intraperitoneally injected along with one third of the treatment. The remaining two-thirds were evenly intraperitoneally administered 2 and 4 days later. The total dose was TRAAb (0.5 mg/kg). For fig. S8, 1×10^6 Nalm-6 cells were intravenously injected 4 days before treatment. On the first day of treatment, all 5×10^6 human T cells were intravenously injected. Treatment here was intravenously injected at 2.5 mg/kg, distributed across five consecutive days. A second infusion of 5×10^6 T cells was also administered on the third day of treatment.

Tumor growth was tracked biweekly using bioluminescent imaging with either the IVIS Ilumina or Spectrum system (PerkinElmer). D-Luciferin substrate (150 μl; Caliper Life Sciences) dissolved at 15 mg/ml in sterile Dulbecco's PBS was intraperitoneally injected 10 min before imaging. Body weight was recorded weekly. Mice were euthanized when bioluminescence total flux reached $>1 \times 10^{10}$ photons/s or earlier if disease symptoms became apparent, including any combination of hunching, swelling, skin color changes, porphyrin staining, and slower behavior. Statistical analysis was performed on day 28 using unpaired t tests, and P values less than 0.05 were considered significant. The averages and SDs shown on the bioluminescent summarized graph correspond to six or seven mice used per group.

Mouse T cell extraction for syngeneic in vitro cytolysis
The fresh spleen was collected from a healthy BALB/c mouse for each experiment, followed by mechanical digestion in sterile PBS supplemented with 2% FBS. A single-cell suspension was prepared using a 70-μm strainer, centrifuged 10 min at 300g and resuspended at $1 \times$ 10^8 cells/ml. A magnetic negative selection kit was then used to purify out T cells (StemCell). Purified T cells were incubated in RPMI (10% FBS and 1% penicillin/streptomycin) at 1×10^6 cells/m per liter overnight before using in cytolysis experiment.

T cell–mediated in vitro syngeneic TRAAb cytolysis
These studies were performed following similar steps as the BiAb studies, except for the following differences. CT26 and 4T1 tumor cells were seeded at 3000 cells per well in 100 μl and incubated 30 min to 1 h before the addition of 25,000 murine T cells in 50 μl and 50 μl of treatments diluted in sterile PBS. TRAAbs and controls were dialyzed in sterile PBS and concentrated using 100 MWCO spin filters (Millipore). TRAAbs and controls were photocrosslinked with a pAbBD fusion that included two copies of the anti-CD3 nanobody. An anti-mouse EGFR antibody conjugated with pAbBD-CD3-CD3 was used as a positive control in the CT26 model (R&D Systems). BALB/c WT control IgG purified from sera was purchased from Innovative Research.

Tissue binding studies using solid syngeneic tumor models
BALB/c mice were subcutaneously injected with 1×10^6 cells. After 14 to 17 days, mice were euthanized and the tumor, liver, spleen, kidney, heart, and lungs were collected. Tissues were fixed in 10% neutral buffered formalin at least 48 hours at 4°C, followed by paraffin embedding and sectioning 10-μm-thick tissues. Fluorescent staining protocols followed those previously reported by Rich et al. (27). Briefly, paraffined sections were treated with xylene, 1:1 mixture of xylene and ethanol, 100% ethanol, 95% ethanol, 70% ethanol, and 50% ethanol 5 min and washed twice 10 min in deionized water. Endogenous peroxidase activity was blocked using stabilized hydrogen peroxide. Blocking was done using a Streptavidin/Biotin kit (Vector Labs), followed by 100% horse serum for 1 hour. CT26 tissues were stained with and without endogenous circulating antibodies as primary antibodies at a concentration of 300 nM, diluted in M.O.M. protein concentrate (Vector Labs). For CT26-HER–positive control, mouse anti-human HER2 (Prestige Antibodies) was used 1:100 diluted in horse serum. Primaries were incubated 2 hours. No primary was used in 4T1 studies. Biotinylated anti-mouse secondary (Vector Labs) was diluted 1:200 in horse serum and incubated 10 min. Biotinylated equine Fab isotype control (Novus Biologicals) was used 1:150 to normalize for technical background in each tissue type. Fluorescent signal was developed using streptavidin–horseradish peroxidase (HRP) and an Alexa Fluor 488 tyramide SuperBoost kit (Invitrogen). Streptavidin-HRP incubation was optimized to 30 min, and the HRP reaction time was optimized to 5 min. All staining steps were done at room temperature. Sections were washed twice for 2 min with PBS between all steps, unless otherwise noted on kits. Stained tissues were mounted using ProLong Diamond antifade (Invitrogen).

Images were acquired using an Olympus IX81 inverted fluorescence microscope and a 4× dry objective. For each tissue section stained, two or three images were obtained and averaged. The images were equalized and normalized against the corresponding tissue signal with nontargeted secondary binding using ImageJ. Statistical analysis was performed using unpaired t tests between the tumor and each other tissue type. All graphs show the mean and SD of three to five mice.

SUPPLEMENTARY MATERIALS

REFERENCES AND NOTES

1. A. F. Labrijn, M. L. Janmaat, J. M. Reichert, P. W. H. I. Parren, Bispecific antibodies: A mechanistic review of the pipeline. *Nat. Rev. Drug Discov.* **18**, 585–608 (2019).

2. F. V. Suurs, M. N. Lub-de Hooge, E. G. E. de Vries, D. J. A. de Groot, A review of bispecific antibodies and antibody constructs in oncology and clinical challenges. *Pharmacol. Ther.* **201**, 103–119 (2019).

3. M. Sebastian, A. Kuemmel, M. Schmidt, A. Schmittel, Catumaxomab: A bispecific trifunctional antibody. *Drugs Today* **45**, 589–597 (2009).

4. R. C. Grabert, L. P. Cousens, J. A. Smith, S. Olson, J. Gall, W. B. Young, P. A. Davol, L. G. Lum, Human T cells armed with Her2/neu bispecific antibodies divide, are cytotoxic, and secrete cytokines with repeated stimulation. *Clin. Cancer Res.* **12**, 569–576 (2006).

5. J. M. Tuscano, Y. Ma, S. M. Martin, J. Kato, R. T. O'Donnell, The Bs20x22 anti-CD20-CD22 bispecific antibody has more lymphomacidal activity than do the parent antibodies alone. *Cancer Immunol. Immunother.* **60**, 771–780 (2011).

6. S. Wang, C. Chen, Y. Meng, S. Hu, L. Zheng, J. Song, D. Zhang, B. Li, Y. Guo, Effective suppression of breast tumor growth by an anti-EGFR/ErbB2 bispecific antibody. *Cancer Lett.* **325**, 214–219 (2012).

7. T. Dreier, P. A. Baeuerle, I. Fichtner, M. Grün, B. Schlereth, G. Lorenczewski, P. Kufer, R. Lutterbüse, G. Riethmüller, P. Gjorstrup, R. C. Bargou, T cell costimulus-independent and very efficacious inhibition of tumor growth in mice bearing subcutaneous or leukemic human B cell lymphoma xenografts by a CD19-/CD3- bispecific single-chain antibody construct. *J. Immunol.* **170**, 4397–4402 (2003).

8. A. Löffler, P. Kufer, R. Lutterbüse, F. Zettl, P. T. Daniel, J. M. Schwenkenbecher, G. Riethmüller, B. Dörken, R. C. Bargou, A recombinant bispecific single-chain antibody, CD19 x CD3, induces rapid and high lymphoma-directed cytotoxicity by unstimulated T lymphocytes. *Blood* **95**, 2098–2103 (2000).

9. R. Bargou, E. Leo, G. Zugmaier, M. Klinger, M. Goebeler, S. Knop, R. Noppeney, A. Viardot, G. Hess, M. Schuler, H. Einsele, C. Brandl, A. Wolf, P. Kirchinger, P. Klappers, M. Schmidt, G. Riethmüller, C. Reinhardt, P. A. Baeuerle, P. Kufer, Tumor regression in cancer patients by very low doses of a T cell–engaging antibody. *Science* **321**, 974–977 (2008).

10. A. Burges, P. Wimberger, C. Kümper, V. Gorbounova, H. Sommer, B. Schmalfeldt, J. Pfisterer, M. Lichinitser, A. Makhson, V. Moiseyenko, A. Lahr, E. Schulze, M. Jäger, M. A. Ströhlein, M. M. Heiss, T. Gottwald, H. Lindhofer, R. Kimmig, Effective relief of malignant ascites in patients with advanced ovarian cancer by a trifunctional anti-EpCAM x anti-CD3 antibody: A phase I/II study. *Clin. Cancer Res.* **13**, 3899–3905 (2007).

11. P. Chames, D. Baty, Bispecific antibodies for cancer therapy: The light at the end of the tunnel? *MAbs* **1**, 539–547 (2009).

12. J. Shen, Z. Zhu, Catumaxomab, a rat/murine hybrid trifunctional bispecific monoclonal antibody for the treatment of cancer. *Curr. Opin. Mol. Ther.* **10**, 273–284 (2008).

13. D. Chelius, P. Ruf, P. Gruber, M. Plöscher, R. Liedtke, E. Gansberger, J. Hess, M. Wasiliu, H. Lindhofer, Structural and functional characterization of the trifunctional antibody catumaxomab. *MAbs* **2**, 301–319 (2010).

14. Q. He, H. Zhang, Y. Wang, H. H. Ting, W. Yu, X. Cao, W. Ge, Purified anti-CD3 × anti-HER2 bispecific antibody potentiates cytokine-induced killer cells of poor spontaneous cytotoxicity against breast cancer cells. *Cell Biosci.* **4**, 70 (2014).

15. A. Krishnamurthy, A. Jimeno, Bispecific antibodies for cancer therapy: A review. *Pharmacol. Ther.* **185**, 122–134 (2018).

16. S. E. Sedykh, V. V. Prinz, V. N. Buneva, G. A. Nevinsky, Bispecific antibodies: Design, therapy, perspectives. *Drug Des. Devel. Ther.* **Volume 12**, 195–208 (2018).

17. C. Gu, D. Ellerman, Production strategies and challenges with IgG-based bispecific Ab formats, in *Development of Biopharmaceutical Drug-Device Products*, F. Jameel, J. W. Skoug, R. R. Nesbitt, Eds. (Springer International Publishing, 2020; https://doi.org/10.1007/978-3-030-31415-6_4), pp. 71–90.

18. S. C. Meyer, C. Huerta, I. Ghosh, Single-site mutations in a hyperthermophilic variant of the B1 domain of protein G result in self-assembled oligomers. *Biochemistry* **44**, 2360–2368 (2005).

19. J. Z. Hui, S. Tamsen, Y. Song, A. Tsourkas, LASIC: Light activated site-specific conjugation of native IgGs. *Bioconjug. Chem.* **26**, 1456–1460 (2015).

20. J. W. Chin, A. B. Martin, D. S. King, L. Wang, P. G. Schultz, Addition of a photocrosslinking amino acid to the genetic code of Escherichia coli. *Proc. Natl. Acad. Sci. U.S.A.* **99**, 11020–11024 (2002).

21. G. Y. K. Ng, S. B. Dixit, T. S. Von Kreudenstein, Bispecific cd3 and cd19 antigen binding contructs, World Patent, (2015); https://patentimages.storage.googleapis.com/81/24/4a/e6a31c17349aa9/WO2015006749A2.pdf.

22. A. Roobrouck, D. Van Hoorick, J. Vieira, T cell recruiting polypeptides based on tcr alpha/beta reactivity. US Patent, US 2019/0112392 A1 (2019); https://patentimages.storage.googleapis.com/74/48/f5/6a8559253279d5/US20190112392A1.pdf.

23. R. Warden-Rothman, I. Caturegli, V. Popik, A. Tsourkas, Sortase-tag expressed protein ligation: Combining protein purification and site-specific bioconjugation into a single step. *Anal. Chem.* **85**, 11090–11097 (2013).

24. J. M. Gall, P. A. Davol, R. C. Grabert, M. Deaver, L. G. Lum, T cells armed with anti-CD3 x anti-CD20 bispecific antibody enhance killing of CD20+ malignant B cells and bypass complement-mediated rituximab resistance in vitro. *Exp. Hematol.* **33**, 452–459 (2005).

25. M. Stanglmaier, M. Faltin, P. Ruf, A. Bodenhausen, P. Schröder, H. Lindhofer, Bi20 (FBTA05), a novel trifunctional bispecific antibody (anti-CD20 x anti-CD3), mediates efficient killing of B-cell lymphoma cells even with very low CD20 expression levels. *Int. J. Cancer* **123**, 1181–1189 (2008).

26. L. L. Sun, D. Ellerman, M. Mathieu, M. Hristopoulos, X. Chen, Y. Li, X. Yan, R. Clark, A. Reyes, E. Stefanich, E. Mai, J. Young, C. Johnson, M. Huseni, X. Wang, Y. Chen, P. Wang, H. Wang, N. Dybdal, Y. W. Chu, N. Chiorazzi, J. M. Scheer, T. Junttila, K. Totpal, M. S. Dennis, A. J. Ebens, Anti-CD20/CD3 T cell-dependent bispecific antibody for the treatment of B cell malignancies. *Sci. Transl. Med.* **7**, 287ra70 (2015).

27. B. S. Rich, J. N. Honeyman, D. G. Darcy, P. T. Smith, A. R. Williams, I. I. P. Lim, L. K. Johnson, M. Gönen, J. S. Simon, M. P. LaQuaglia, S. M. Simon, Endogenous antibodies for tumor detection. *Sci. Rep.* **4**, 5088 (2014).

28. J. Z. Hui, A. A. Zaki, Z. Cheng, V. Popik, H. Zhang, E. T. Luning Prak, A. Tsourkas, Facile method for the site-specific, covalent attachment of full-length IgG onto nanoparticles. *Small* **10**, 3354–3363 (2014).

29. J. Z. Hui, A. Tsourkas, Optimization of photoactive protein Z for fast and efficient site-specific conjugation of native IgG. *Bioconjug. Chem.* **25**, 1709–1719 (2014).

30. A. DiGiandomenico, A. E. Keller, C. Gao, G. J. Rainey, P. Warrener, M. M. Camara, J. Bonnell, R. Fleming, B. Bezabeh, N. Dimasi, B. R. Sellman, J. Hilliard, C. M. Guenther, V. Datta, W. Zhao, C. Gao, X.-Q. Yu, J. A. Suzich, C. K. Stover, A multifunctional bispecific antibody protects against *Pseudomonas aeruginosa*. *Sci. Transl. Med.* **6**, 262ra155 (2014).

31. Z. B. Davis, T. Lenvik, L. Hansen, M. Felices, S. Cooley, D. Vallera, A. T. Haase, R. A. Koup, D. Douek, T. Schacker, J. S. Miller, A novel HIV envelope Bi-specific killer engager enhances natural killer cell mediated ADCC responses against HIV-infected cells. *Blood* **128**, 2517–2517 (2016).

32. A. Beck, L. Goetsch, C. Dumontet, N. Corvaïa, Strategies and challenges for the next generation of antibody–drug conjugates. *Nat. Rev. Drug Discov.* **16**, 315–337 (2017).

33. H. H. Wang, B. Altun, K. Nwe, A. Tsourkas, Proximity-based sortase-mediated ligation. *Angew. Chem. Int. Ed. Engl.* **56**, 5349–5352 (2017).

34. G. P. Adams, L. M. Weiner, Monoclonal antibody therapy of cancer. *Nat. Biotechnol.* **23**, 1147–1157 (2005).

35. C. J. Chapman, A. Murray, J. E. McElveen, U. Sahin, U. Luxemburger, O. Türeci, R. Wiewrodt, A. C. Barnes, J. F. Robertson, Autoantibodies in lung cancer: Possibilities for early detection and subsequent cure. *Thorax* **63**, 228–233 (2008).

36. A. Fosså, A. Berner, S. D. Fosså, E. Hernes, G. Gaudernack, E. B. Smeland, NY-ESO-1 protein expression and humoral immune responses in prostate cancer. *Prostate* **59**, 440–447 (2004).

37. F. Korangy, L. A. Ormandy, J. S. Bleck, J. Klempnauer, L. Wilkens, M. P. Manns, T. F. Greten, Spontaneous tumor-specific humoral and cellular immune responses to NY-ESO-1 in hepatocellular carcinoma. *Clin. Cancer Res.* **10**, 4332–4341 (2004).

38. M. Maio, S. Coral, L. Sigalotti, R. Elisei, C. Romei, G. Rossi, E. Cortini, F. Colizzi, G. Fenzi, M. Altomonte, A. Pinchera, M. Vitale, Analysis of cancer/testis antigens in sporadic medullary thyroid carcinoma: Expression and humoral response to NY-ESO-1. *J. Clin. Endocrinol. Metab.* **88**, 748–754 (2003).

39. Y. Merbl, R. Itzchak, T. Vider-Shalit, Y. Louzoun, F. J. Quintana, E. Vadai, L. Eisenbach, I. R. Cohen, A systems immunology approach to the host-tumor interaction: Large-scale patterns of natural autoantibodies distinguish healthy and tumor-bearing mice. *PLOS ONE* **4**, e6053 (2009).

40. P. J. Mintz, J. Kim, K.-A. Do, X. Wang, R. G. Zinner, M. Cristofanilli, M. A. Arap, W. K. Hong, P. Troncoso, C. J. Logothetis, R. Pasqualini, W. Arap, Fingerprinting the circulating repertoire of antibodies from cancer patients. *Nat. Biotechnol.* **21**, 57–63 (2003).

41. E. Stockert, E. Jäger, Y. T. Chen, M. J. Scanlan, I. Gout, J. Karbach, M. Arand, A. Knuth, L. J. Old, A survey of the humoral immune response of cancer patients to a panel of human tumor antigens. *J. Exp. Med.* **187**, 1349–1354 (1998).

42. P. Zaenker, E. S. Gray, M. R. Ziman, Autoantibody production in cancer—The humoral immune response toward autologous antigens in cancer patients. *Autoimmun. Rev.* **15**, 477–483 (2016).

43. W.-X. Chen, X.-B. Hong, C.-Q. Hong, M. Liu, L. Li, L.-S. Huang, L.-Y. Xu, Y.-W. Xu, Y.-H. Peng, E.-M. Li, Tumor-associated autoantibodies against Fascin as a novel diagnostic biomarker for esophageal squamous cell carcinoma. *Clin. Res. Hepatol. Gastroenterol.* **41**, 327–332 (2017).

44. T. Wang, M. Liu, S.-J. Zheng, D.-D. Bian, J.-Y. Zhang, J. Yao, Q.-F. Zheng, A.-M. Shi, W.-H. Li, L. Li, Y. Chen, J.-H. Wang, Z.-P. Duan, L. Dong, Tumor-associated autoantibodies are useful biomarkers in immunodiagnosis of α-fetoprotein-negative hepatocellular carcinoma. *World J. Gastroenterol.* **23**, 3496–3504 (2017).

45. Z.-M. Tang, Z.-G. Ling, C.-M. Wang, Y.-B. Wu, J.-L. Kong, Serum tumor-associated autoantibodies as diagnostic biomarkers for lung cancer: A systematic review and meta-analysis. *PLOS ONE* **12**, e0182117 (2017).

46. V. Tolmachev, A. Orlova, Affibody molecules as targeting vectors for PET imaging. *Cancers* **12**, 651 (2020).

47. S. Ståhl, T. Gräslund, A. Eriksson Karlström, F. Y. Frejd, P.-Å. Nygren, J. Löfblom, Affibody molecules in biotechnological and medical applications. *Trends Biotechnol.* **35**, 691–712 (2017).

48. F. Y. Frejd, K.-T. Kim, Affibody molecules as engineered protein drugs. *Exp. Mol. Med.* **49**, e306 (2017).

49. S. Ge, J. Li, Y. Yu, Z. Chen, Y. Yang, L. Zhu, S. Sang, S. Deng, Review: Radionuclide molecular imaging targeting HER2 in breast cancer with a focus on molecular probes into clinical trials and small peptides. *Molecules* **26**, 6482 (2021).

50. S. Borghi, S. Bournazos, N. K. Thulin, C. Li, A. Gajewski, R. W. Sherwood, S. Zhang, E. Harris, P. Jagannathan, L.-X. Wang, J. V. Ravetch, T. T. Wang, FcRn, but not FcγRs, drives maternal-fetal transplacental transport of human IgG antibodies. *Proc. Natl. Acad. Sci. U.S.A.* **117**, 12943–12951 (2020).

51. P. Bruhns, B. Iannascoli, P. England, D. A. Mancardi, N. Fernandez, S. Jorieux, M. Daëron, Specificity and affinity of human Fcgamma receptors and their polymorphic variants for human IgG subclasses. *Blood* **113**, 3716–3725 (2009).

52. K.-D. Preuss, C. Zwick, C. Bormann, F. Neumann, M. Pfreundschuh, Analysis of the B-cell repertoire against antigens expressed by human neoplasms. *Immunol. Rev.* **188**, 43–50 (2002).

53. Q. Zhu, M. Liu, L. Dai, X. Ying, H. Ye, Y. Zhou, S. Han, J.-Y. Zhang, Using immunoproteomics to identify tumor-associated antigens (TAAs) as biomarkers in cancer immunodiagnosis. *Autoimmun. Rev.* **12**, 1123–1128 (2013).

54. J. Y. Zhang, W. Zhu, H. Imai, K. Kiyosawa, E. K. Chan, E. M. Tan, De-novo humoral immune responses to cancer-associated autoantigens during transition from chronic liver disease to hepatocellular carcinoma. *Clin. Exp. Immunol.* **125**, 3–9 (2001).

55. N. G. Minutolo, P. Sharma, M. Poussin, L. C. Shaw, D. P. Brown, E. E. Hollander, A. Smole, A. Rodriguez-Garcia, J. Z. Hui, F. Zappala, A. Tsourkas, D. J. Powell Jr., Quantitative control of gene-engineered T-cell activity through the covalent attachment of targeting ligands to a universal immune receptor. *J. Am. Chem. Soc.* **142**, 6554–6568 (2020).

56. S. Liu, R. Tobias, S. McClure, G. Styba, Q. Shi, G. Jackowski, Removal of endotoxin from recombinant protein preparations. *Clin. Biochem.* **30**, 455–463 (1997).